THE BALTIC JOURNAL
OF ROAD AND BRIDGE ENGINEERING
2025/20(1)

SSN 1822-427X/eISSN 1822-4288
2025 Volume 20 Issue 1: 45–69
https://doi.org/10.7250/bjrbe.2025-20.653

QUANTITATIVE EVALUATION OF INTERNAL PAVEMENT DISTRESSES BASED ON 3D GROUND PENETRATING RADAR

YONG LIU[1], ZHIWEN ZHANG[1], YANG YUAN[2], YUNSHENG ZHU[2*], KAIFENG WANG[2]

[1]*Wuhan CCCC Test, Detection and Reinforcement Engineering Co., Ltd, Wuhan 430050, China*
[2]*School of Transportation and Logistics Engineering, Wuhan University of Technology, Wuhan 430063, China*

Received 3 June 2024; accepted 29 January 2025

Abstract. Asphalt pavement will inevitably produce internal distresses during service, which increases the risk of deterioration of pavement structural performance. Although three-dimensional ground penetrating radar (3D GPR) with a multi-channel antenna array can detect the internal structural condition of asphalt pavement non-destructively and quickly, there is currently a lack of effective evaluation index and standard. In this paper, 3D GPR was used to investigate four typical internal distresses of existing asphalt pavement in Guangzhou-Shaoguan Expressway, including cracks, loose, cavities, and poor interlayer bonding. In particular, GprMax software was used to establish the quantitative relationship between base crack width and radar images. Based on the radar image characteristics of different internal distresses, the distresses at the asphalt layer, base, and subbase were identified and statistically analysed. Pavement internal condition index (PICI) was proposed to quantitatively assess the internal distress condition of asphalt pavement. The results show that the PICI based on 3D GPR is reliable for evaluating the internal distress condition of pavement structure, and

* Corresponding author. E-mail: zhuyunshengwhlgdx@163.com

Yang YUAN (ORCID ID 0000-0003-0690-568X)
Yunsheng ZHU (ORCID ID 0000-0002-7145-5446)

can be used as an important supplementary part of pavement structural integrity evaluation. The evaluation results can provide a reference for asphalt pavement maintenance decision.

Keywords: asphalt pavement, evaluation index, ground penetrating radar, internal distress, maintenance measures, radar image.

Introduction

Currently, China's highway network is becoming more and more mature and has gradually entered a large-scale maintenance period. With the continuous increase of traffic volume, asphalt pavement is prone to produce more distresses, including road surface distresses (such as ruts, cracks) and internal distresses (such as cavitation, voids) under the dual action of traffic load and environmental factors (Hernando & del Val, 2013; Xiong et al., 2024a). Once there is hidden distress inside the pavement, it will be exposed to the surface quickly under the action of load, resulting in reflective cracks, subsidence, thus affecting the safety and comfort of driving. For maintenance engineering, the road condition detection vehicle is generally used to investigate the pavement surface distress. China's current Highway Performance Assessment Standard (JTG 5210 H20-2018) stipulates five technical indicators for asphalt pavement performance evaluation, including the pavement condition index (PCI), riding quality index (RQI), rutting depth index (RDI), skidding resistance index (SRI), and pavement structural strength index (PSSI) (Jing et al., 2020; Iftikhar et al., 2023). These indicators mainly evaluate the condition of the road surface and lack indicators for evaluating distresses within the pavement. The detection of pavement internal distresses is mainly based on the destructive approach, a direct appreciation of the type of structural distress through the coring of the pavement, which is difficult to comprehensively evaluate the condition of pavement internal structure (Kırbaş & Karaşahin, 2016). According to the investigation of the quality of asphalt pavement, it is found that the road surface distresses is closely related to the hidden distresses of the pavement internal structure, which has aroused the attention of the maintenance department (Obaidat & Al-Kheder, 2006; Farhan et al., 2018). Therefore, for the semi-rigid base asphalt pavement, the comprehensive performance evaluation of the in-service pavement should include more effective indicators not only referring to the asphalt layer but also base. Non-destructive testing and quantitative evaluation of the pavement internal distress is an urgent need for highway development.

At present, ground penetrating radar (GPR) has already shown superiority in road engineering detection for its non-destructive and high efficiency. GPR is increasingly reliable for pavement performance assessment, including the detection of thickness and compactness of asphalt pavement, quality control of the newly constructed highway, detecting the voids and cracks in pavement, etc. (Xiong

and Tan, 2023). In the detection of internal pavement distress, the traditional 2D GPR is limited by the antenna frequency, which has problems such as a long identification period and low efficiency (Xiong et al., 2021). In addition, 2D GPR can only provide vertical profile, which is able to identify the approximate location of the pavement structure internal distress, but cannot quantitatively describe the three-dimensional spatial location and size (Diamanti & Redman, 2012; Joshaghani & Shokrabadi, 2022). Over the past decade, the rapid development of 3D GPR based on antenna array technology has opened up a new space for road detection. Compared to the 2D GPR, 3D GPR is able to collect the full structure data of a pavement section. Informative 3D data can be used to detect internal pavement distress, such as cracks, voids, poor interlayer bonding, and mixture segregation (Lai et al., 2018). For example, Li et al. (2021) detected road cracks using 3D GPR, and determined the morphology and development horizon of cracks according to radar profile images at different depths. Giannakis et al. (2019) built a radar graph spectrum of pavement internal distresses by extracting typical features from radar images, including looseness, cavities and water-rich zones. Muller (2020) proposed an air voids content measurement method for asphalt pavement based on 3D GPR, which has a certain guiding role for construction quality control. Leng et al. (2014) proposed a pavement distress detection model based on extended common central point method, which is helpful for road maintenance decision-making. In a word, 3D GPR has become the most commonly used and comparatively most efficient pavement distress detection and evaluation technique. Unfortunately, the current research focuses on finding internal distresses through advanced non-destructive testing technology, but there is not much work on the quantitative evaluation of pavement structural integrity.

In this paper, 3D GPR is used to detect the internal pavement distress, and its accuracy is verified by onsite coring of the distress. Based on the obtained clear three-dimensional radar images, three-dimensional internal distress ratio (IDR) and pavement internal condition index (PICI) are established by extracting the size information of distress from the images. In this process, considering that the width cannot be accurately extracted from the radar image of the crack, using GprMax, GPR forward modelling toward base cracks is conducted to investigate the relationship between the dimension of the crack and the feature of its radar image. The PICI model based on 3D GPR implements the quantitative evaluation of the pavement internal structure distress, which provides a basis for making pavement maintenance plan.

1. Methodology

According to Chinese specification, the common detection methods for asphalt pavement surface distresses are artificial walking survey and multi-function vehicle. By recording the type, quantity, and severity of surface distress, the distress rate

(DR) and pavement condition index (PCI) are calculated using Equations (1) and (2) (Zhou et al., 2014). The PCI is a numerical rating of pavement condition ranging from 0 to 100, with a value greater than 90 indicating good condition and a value less than 60 indicating poor condition.

$$DR = 100 \times \frac{\sum_{i=1}^{i_0} w_i A_i}{A}, \tag{1}$$

$$PCI = 100 - a_0 DR^{a_1}, \tag{2}$$

where A_i – area of the i-type distress, m^2;
A – area of survey pavement, m^2;
w_i – weight of the i-type distress (value range 0–1);
a_0 and a_1 – adjustment factor;
i_0 – total number of distress types.
For asphalt pavement, $a_0 = 15$, $a_1 = 0.412$, and $i_0 = 21$.

However, the China's latest Specifications for Maintenance Design of Highway Asphalt Pavement (JTG 5421 H20-2018) emphasise structural integrity detection. The PCI can only represent the damage condition of the pavement surface and cannot effectively guide the maintenance of the pavement internal structure. Therefore, IDR and PICI were proposed to evaluate the pavement internal distress based on PCI model, as shown in Equations (3) and (4). The PICI model characterises the internal distress state from a full spatial perspective (depth, longitudinal, and transverse), which can truly reflect the damage condition of the pavement internal structure, and is suitable for evaluating the structural layer integrity of asphalt pavement. In practical applications, high-quality 3D GPR image data of pavement structure is the prerequisite for the calculation of these three-dimensional parameters. According to the characteristics of 3D radar images of pavement internal distresses (Liang et al., 2022), the PICI model only considers four types of internal distresses, namely crack, loose, cavity, and poor interlayer bonding, as detailed in Section 4. Meanwhile, there are great differences in the influence of different types of pavement internal distresses on structural strength, such as poor interlayer bonding has less impact, but cavity has a greater impact. Therefore, according to this influence relationship, the weights of each internal distress were determined, as shown in Table 1. Since it is difficult for GPR to detect minor internal damage, pavement internal distresses are all uniformly treated as serious distresses (Xiong et al., 2024b). The evaluation criteria of PICI model are shown in Table 2.

$$IDR = 100 \times \frac{\sum_{j=1}^{j_0} w_j A_j h_j}{A \times H}, \tag{3}$$

$$PICI = 100 - a_0 \times IDR^{a_1}, \tag{4}$$

where h_j – extension depth of the j-type internal distress, m;
H – total thickness of the pavement structure, m;
j_0 – total number of internal distress types.
Considering the change in dimension, a_0 and a_1 are adjusted from 15 and 0.412 to 14.824 and 0.564.

Table 1. Internal distress types and weights of asphalt pavement

Type (j)	Distress	Weight (w_j)
1	Crack	0.5
2	Loose	0.8
3	Cavity	1.0
4	Poor interlayer bonding	0.3

Table 2. Evaluation criteria of PICI model

Evaluation grade	I	II	III	IV
IDR, %	≤ 0.54	(0.54, 1.61]	(1.61, 3.54]	> 3.54
PICI	≥ 90	[80, 90)	[70, 80)	< 70

2. The principle and composition of 3D GPR

2.1. Detection principle

3D GPR transmits high-frequency pulsed electromagnetic waves into the pavement using an antenna (Baili et al., 2009). When the electromagnetic wave encounters the stratum or the object with different electrical properties, it will be reflected and refracted. The refracted electromagnetic waves continue to propagate downward, while the reflected electromagnetic waves carrying information are received by the antenna. The echo signal is analysed by the signal processor to generate a wave-form scan line. When the GPR moves along the detection line,

multiple scan lines are collected. Then, the visual radar image can be obtained by splicing these scanning lines. The spatial position, structure and shape of the underground medium can be deduced by analysing the waveform, amplitude intensity and time change of the electromagnetic wave signal received by the radar system. The detection principle is shown in Figure 1.

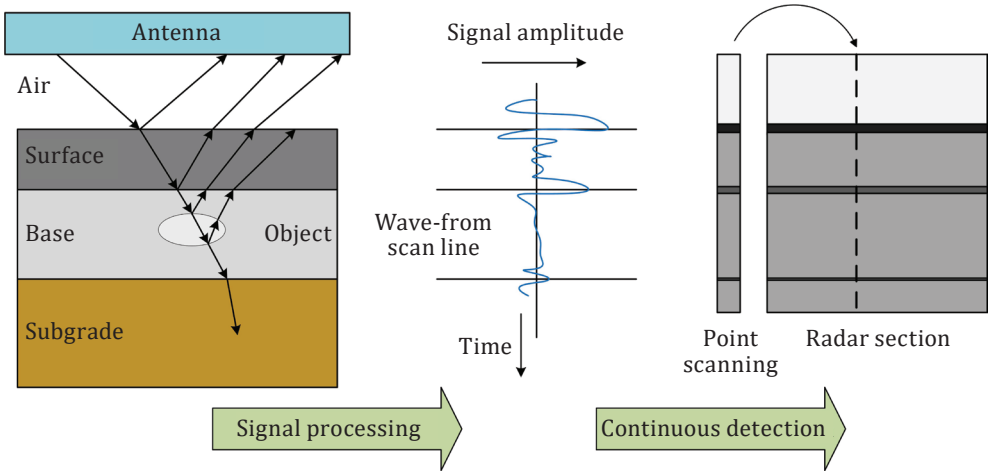

Figure 1. The diagram of GPR detection principle

The reflection and refraction characteristics of electromagnetic wave at the interface of different media layers are related to the dielectric constant, and the change law of wave-form and amplitude is determined by the reflection coefficient, as shown in Equation (5) (Benedetto et al., 2017). Obviously, for the pavement structure without distress, the reflection coefficient of the reflected wave at the same layer is 0. A large number of continuous reflected waves with the same phase appear as horizontal linear distributions on radar images, which are called in-phase axes (dark part in Figure 1). On the contrary, for the structure layer with distress, due to the great difference between the dielectric constant of the distress and the surrounding normal pavement material, the phenomenon of bending, interruption and clutter of the in-phase axis will appear in the radar image.

$$R = \frac{\sqrt{\varepsilon_1} - \sqrt{\varepsilon_2}}{\sqrt{\varepsilon_1} + \sqrt{\varepsilon_2}}, \tag{5}$$

where R – reflection coefficient;
ε_1 – dielectric constant of the upper media;
ε_2 – dielectric constant of the lower media.

2.2. 3D-radar system

GeoScope 3D GPR system produced by Norwegian 3D-Radar Company was used to collect data, mainly including GeoScope™ MK IV radar mainframe, DXG1820 ground-coupled antenna array, RT3D acquisition software, and 3dr-Examiner data processing software, as shown in Figure 2. The distance-measuring instrument (DMI) is fixed on the rear wheel to track the movement path of the radar antenna. The real-time kinematic (RTK) on the antenna is used to improve the accuracy and efficiency of the detection.

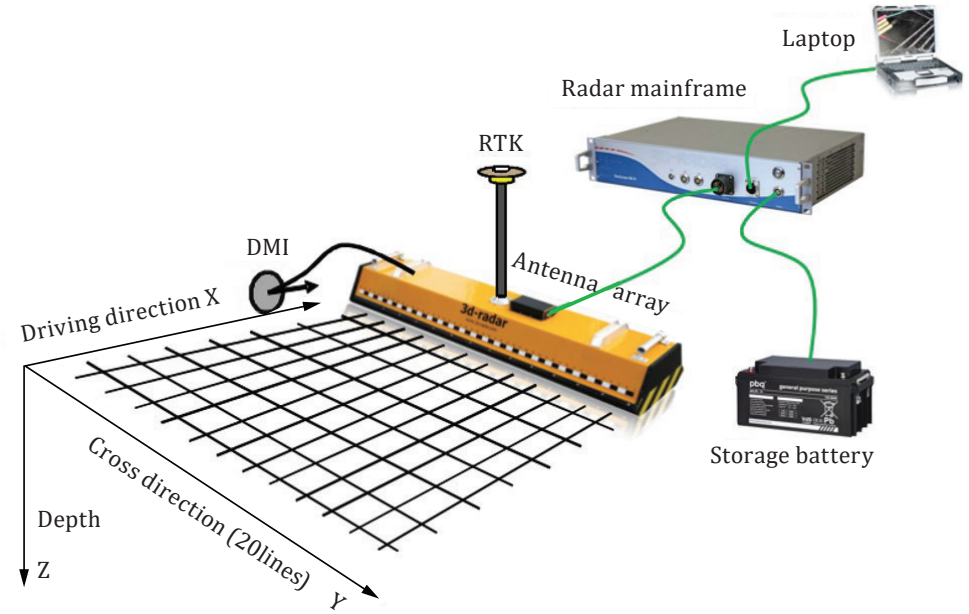

Figure 2. Components of ground-coupled 3D GPR system

The main features of 3D GPR are the use of stepped-frequency, antenna array, and three-dimensional imaging technology. The stepped-frequency antenna has a scanning range of 100 MHz to 3 GHz and is capable of continuous linear frequency scanning of up to 1500 steps at wavelengths from 0.5 ms to 10 ms, as shown in Figure 3. The 2900 MHz ultra-bandwidth allows for the resolution to reach 0.34 ns, and the detection depth can reach 2 to 3 m. Moreover, stepped-frequency technology enables a balance between depth and resolution to be achieved in one detection. By setting the frequency of the transmitting antenna, the user can obtain the best resolution image in the detection depth range.

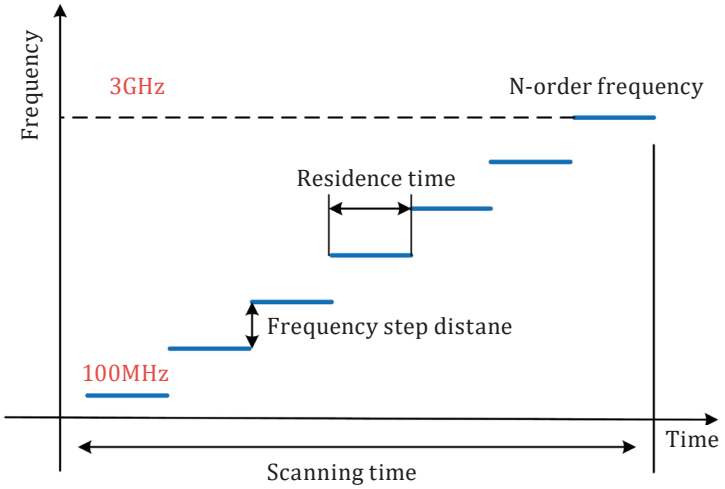

Figure 3. Stepped-frequency principle

The DXG1820 antenna array contains 20 pairs of electronic scanning antenna oscillators, which can simultaneously collect radar data of 20 channels. The spacing of the antenna array is 7.5 cm, and the width of one detection scan can reach 1.5 m. In addition, the 3D GPR antenna system adopts the method of separating transmit antenna (T) and receive antenna (R) and equidistant staggered arrangement, which achieves the ideal state of the profile spacing close to 1/4 wavelength of the antenna centre frequency (Liu & Sato, 2014), as shown in Figure 4. Compared to 2D GPR, the detection efficiency is greatly improved.

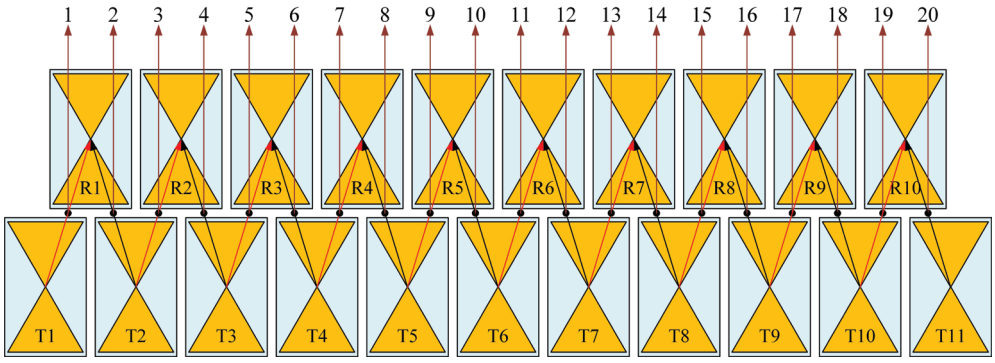

Figure 4. Layout of the DXG1820 antenna array

The RT3D acquisition software can obtain the detailed information of longitudinal section, cross section, and horizontal section within the pavement structure in real time. After processing this information in the 3dr-Examiner software, the radargram of three dimensions (X, Y, and Z) are clearly displayed in the window, as depicted in Figure 5. As can be seen from Figure 5(a), it shows that the 3D GPR can output detection images of three views: B-Scan, C-Scan, and D-Scan. Due to the obvious difference in the dielectric contrast of different structural layers, the inline slice in Figure 5(b) presents three distinct in-phase axes, namely the interfaces between structural layers. In addition, there are two blue straight lines in each section. The high-resolution images of any underground position can be obtained by moving the blue line, which implements the rapid detection and accurate positioning of the internal distresses of pavement.

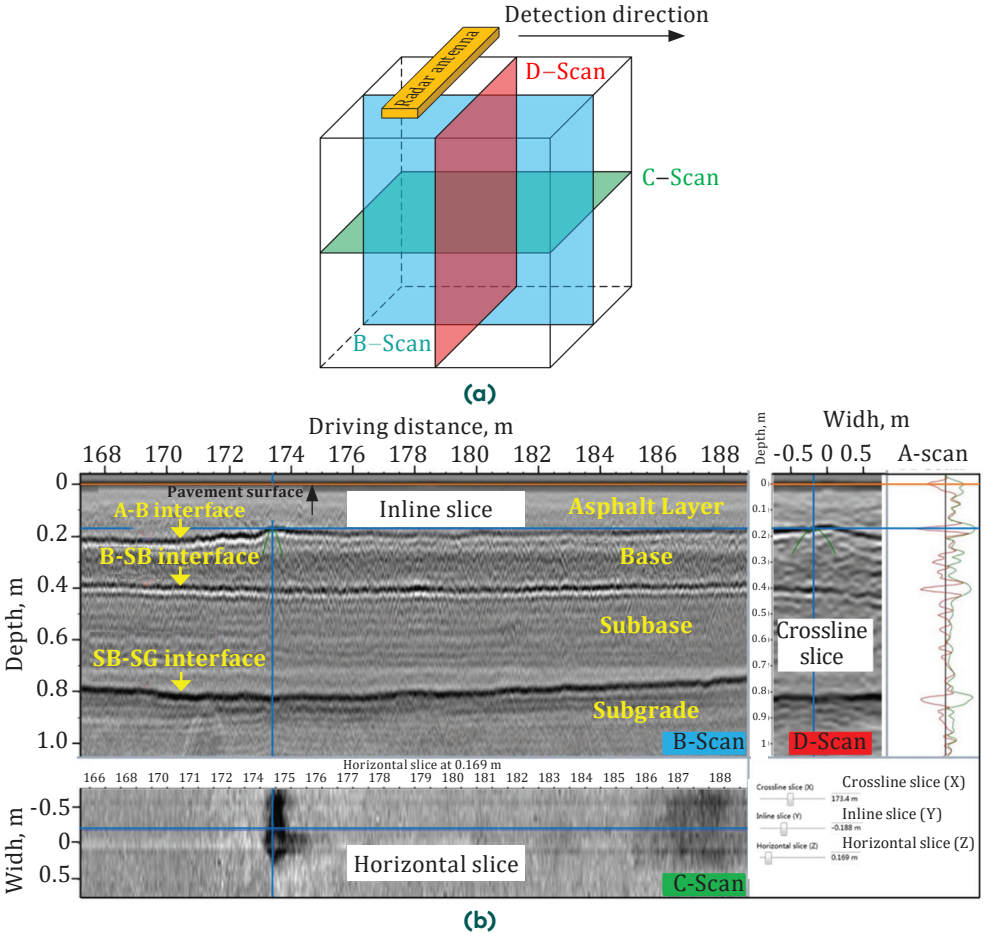

Figure 5. 3D GPR image acquisition: (a) – three views of radar detection; (b) – detection images corresponding to three-dimensional views

3. 3D GPR investigation of internal distresses in asphalt pavement

3.1. Features of internal distresses in GPR images

The pavement internal distresses considered in the PICI model are cracks, loose, cavities, and poor interlayer bonding. The typical characteristics of each internal distress in radar images are shown in Table 3. Different distresses were represented clearly in the longitudinal and horizontal radar images. Therefore, longitudinal and horizontal radar images provide a unique perspective for pavement distress quantification and can be used as a powerful basis for PICI evaluation.

Table 3. Radar image features of different pavement internal distress
(table continues on the next page)

Distress	B-Scan (longitudinal section)	C-Scan (horizontal section)	Features
Crack	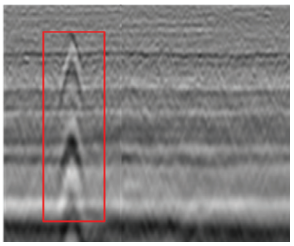	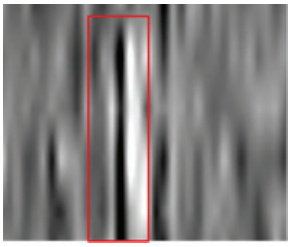	An obvious hyperbolic feature in B-Scan, and a dark long stripe in C-Scan.
Loose	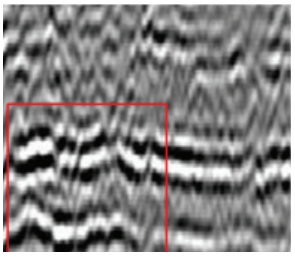	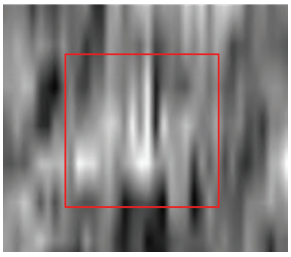	A messy waveform feature in B-Scan, and many scattered highlighted areas in C-Scan.

Table 3 (continue). Radar image features of different pavement internal distress

Distress	B-Scan (longitudinal section)	C-Scan (horizontal section)	Features
Cavity	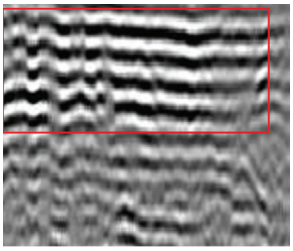	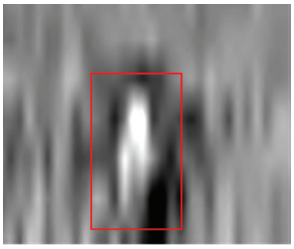	A bright irregular reflection band feature in B-Scan, and a black-and-white highlighted area in C-Scan.
Poo nterlayer bonding	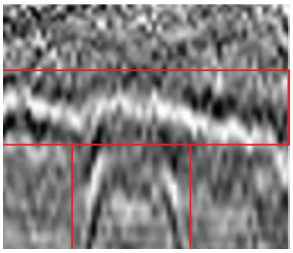	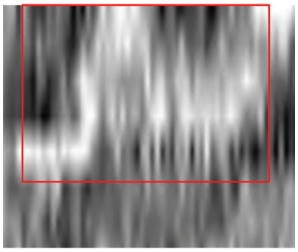	An abnormal signal accompanied by diffraction wave feature in B-Scan, and a large-scale highlight anomaly in C-Scan.

3.2. Detection of road internal distress by 3D GPR

The detected road is the Guangzhou-Shaoguan (Guang-Shao) Expressway in Guangdong Province, China. In 2020, the special repair of pavement was carried out on the Guang-Shao Expressway. However, after only two years, the maintenance area of road started to show a rapid growth trend. In order to develop a reliable and targeted pavement distress maintenance scheme for the Guang-Shao Expressway, the structural performance of Guang-Shao Expressway needs to be fully evaluated. Therefore, 3D GPR was used to detect the right three-lane roadway structure internal distress of the highway, and the length of the detected section was 2.5 km (mile stake K2117 + 000 ~ K2119 + 500), as shown in Figure 6. The total thickness H of pavement structure is 0.9 m. Since the lane width is 3.75 m, two scan lines are arranged in one lane to detect the whole lane as much as possible. Lane 1 is the overtaking lane near the median divider, lane 2 is the middle lane, and lane 3 is the slow lane near the hard shoulder.

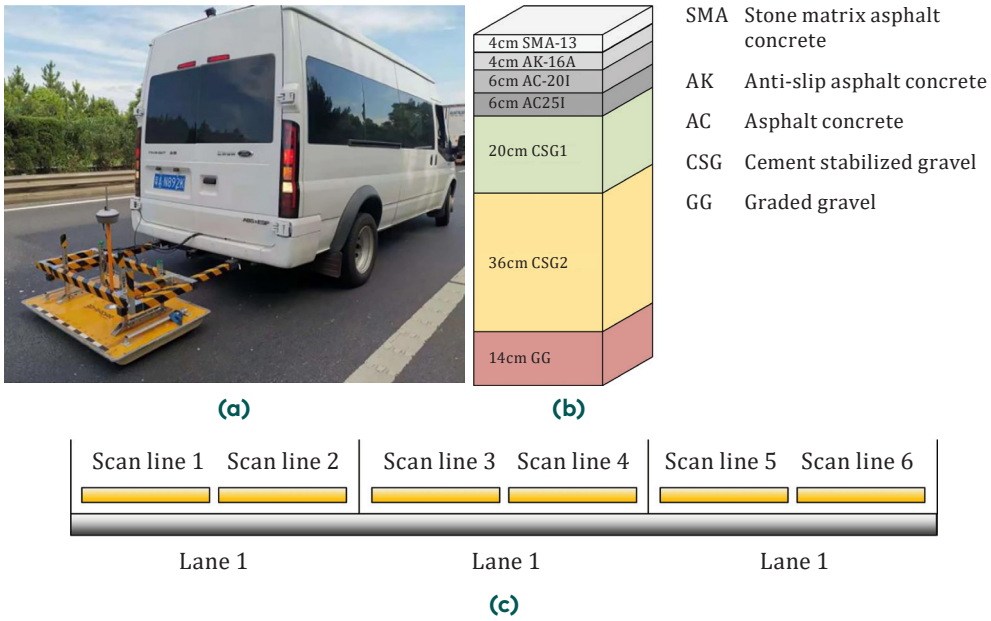

Figure 6. Field detection of 3D GPR: (a) – 3D GPR equipment; (b) – pavement structure; (c) – detection way

In Figure 7, 3D GPR images of poor bonding are presented at asphalt layer interface. The radar signal on the inline slice has a relatively strong reflection signal in the area between the layers, and there is a bright area on the horizontal slice which is significantly different from the surrounding area. Field core sample also showed that the pavement structural layers were good overall, but the bond between the layers was poor. There is a bright area in the horizontal slice that is significantly different from the surrounding area, and the distress area A can be calculated using image processing technology. The extension depth h of the distress can be obtained by moving the horizontal blue line up and down in the inline slice and simultaneously observing the changes of the distress in the horizontal slice. Figure 8 shows the horizontal slices and corresponding core samples of crack, loose, and cavity at specific depth, respectively. It can be seen that the corresponding relationship between the 3D GPR image and the field core sample is obvious. The 3D GPR can accurately identify and detect the internal distress condition of the road.

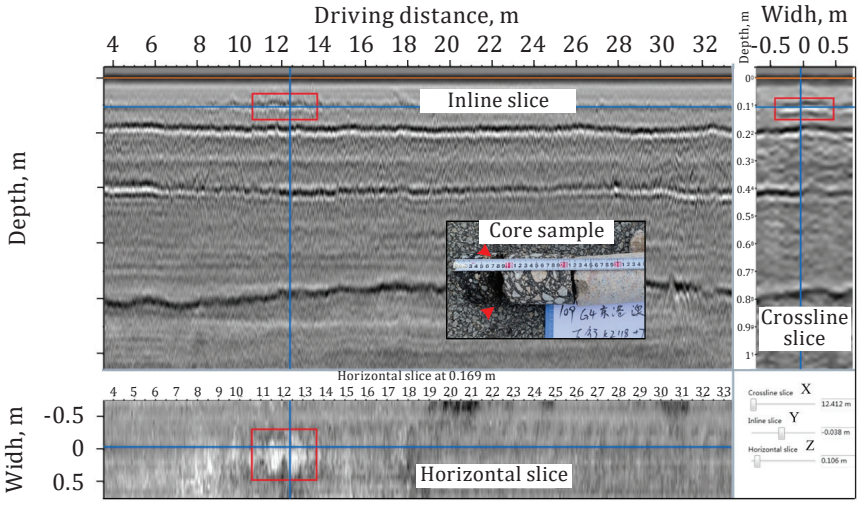

Figure 7. 3D radargram of poor bonding at asphalt layer interface

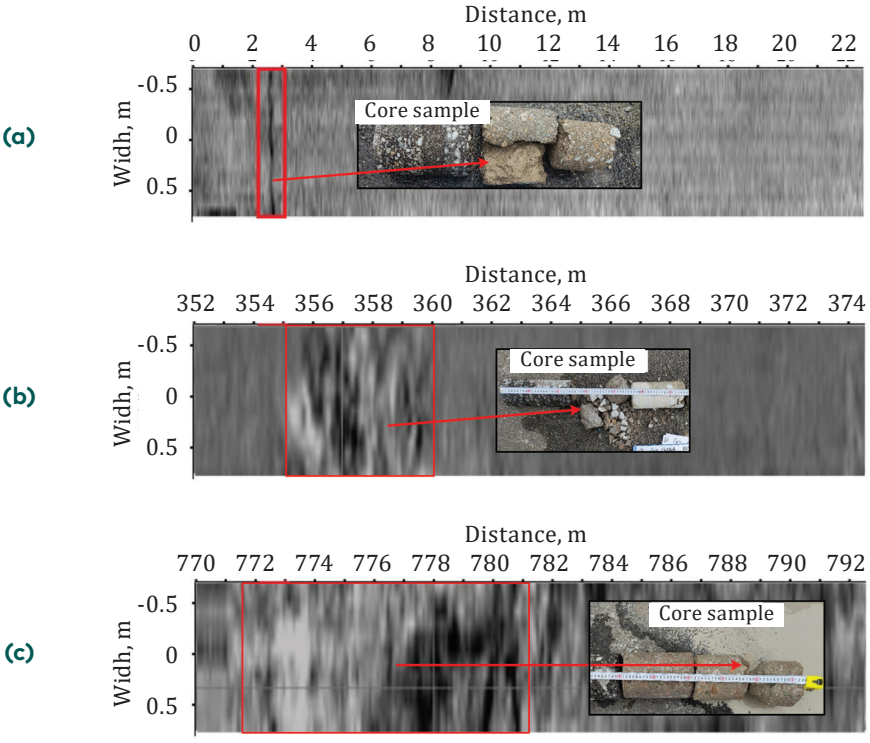

Figure 8. Horizontal slices and corresponding core samples of pavement internal distress: (a) – crack at 0.175 m depth; (b) – loose at 0.195 m depth; (c) – cavity at 0.385 m depth

4. Forward modelling toward a base crack

It can be seen from Table 2 that the crack shows an obvious hyperbolic characteristic on the radar profile. Therefore, in this section, GprMax software is used for GPR forward modelling of base cracks to investigate the relationship between crack width and echo signal.

4.1. Basic model

GprMax 3.0 is a three-dimensional forward simulation software for ground-penetrating radar based on the finite difference time domain method (Feng et al., 2013). Building the model for numerical simulation is based on the following assumptions: 1) the materials of the medium in the model are isotropic; 2) the electrical properties of the materials are not affected by the frequency change; 3) the depth direction is a continuous extension in space without boundaries (Liu et al., 2023).

In order to be consistent with the radar images obtained by GeoScope 3D Radar, the road model structure refers to the pavement structure of Guang-Shao Expressway. The thickness of pavement structure layer is set at 0.9 m, which consists of 20 cm asphalt concrete surface layer with a relative permittivity of 6, 20 cm cement stabilised macadam base with a relative permittivity of 10, 36 cm low-dose cement stabilised macadam subbase with a relative permittivity of 8, and 14 cm soil subgrade with a relative permittivity of 12. The radar excitation source is located in the surface layer, and the upper free space is 80 cm air layer, which can reduce the interference effect of electromagnetic wave on detection. The schematic diagram of the model is shown in Figure 9. Since pavement materials are non-magnetic, the relative permeability is taken as 1. The materials are also non-conductive, so the conductivity is taken as 0.005. Referring to the characteristics of DXG1820 antenna array, the related parameters of the model are shown in Table 4. Besides, a 2 cm thick PML (perfectly matched layer) absorption boundary condition is set around the model, so that the reflection of the electromagnetic wave will only happen where the permittivity changes.

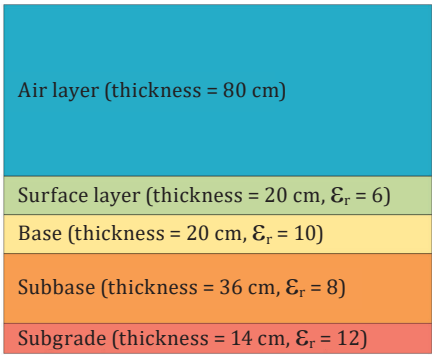

Figure 9. The diagram of the basic model

Table 4. Parameters of GPR forward simulation

Parameter	Value
Model size, m	
2.0 × 1.7	
Space grid step size, m	0.002 × 0.002
Time window, ns	20
Initial transmitting antenna coordinate, m	(0.02, 0.88)
Initial receiving antenna coordinate, m	(0.17, 0.88)
Antenna step length, m	0.01
Excitation source type	Ricker
Excitation source frequency, MHz	900

4.2. Influence of the crack width on its radar echo

As the width of a base crack is generally between 1 and 20 mm (Wang et al., 2008), the width of cracks in those models is set to 2, 6, 10, 15, 20, and 25 mm, respectively. Considering the actual conditions of the pavement, these cracks are all through cracks. Figure 10 shows the series of models with a single crack of different widths (combined into one image for comparison). After forward modelling toward these models, the direct coupled wave in the original image is removed to get clearer results, as shown in Figure 11.

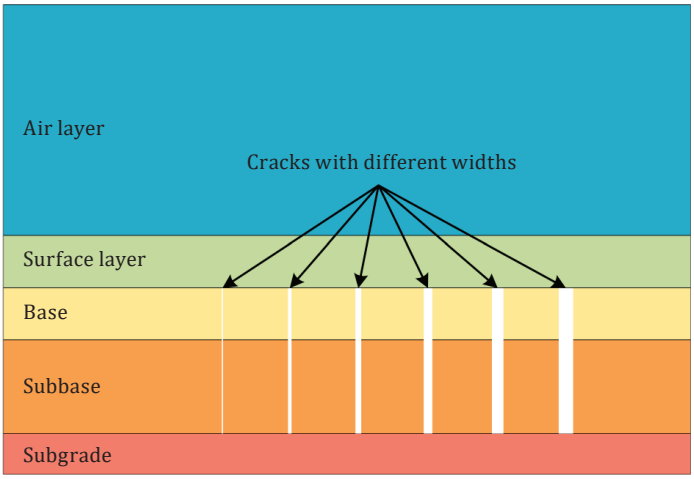

Figure 10. Models with a crack of different widths

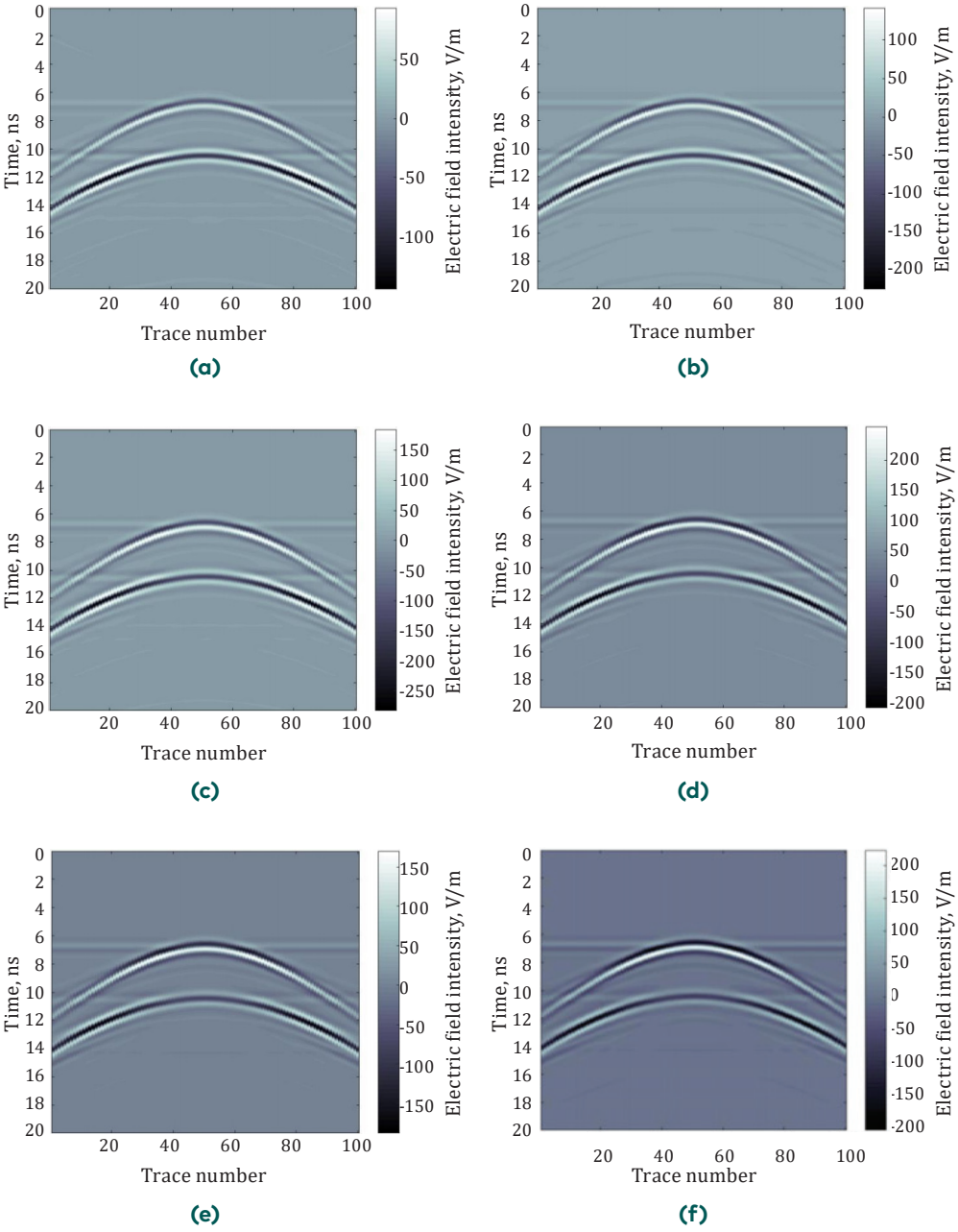

Figure 11. Results of forward modelling toward models with a crack of different widths: (a) – 2 mm; (b) – 6 mm; (c) – 10 mm; (d) – 15 mm; (e) – 20 mm; (f) – 25 mm

The shape of the crack echo is almost invariant under the change of width, indicating that the crack width does not affect the waveform of the radar image. However, the echo amplitude has a pretty clear relationship with the crack width, namely the larger the crack width, the larger the echo amplitude. To further quantify this correlation, the echo amplitude at the top of the crack, that is, the peak value of reflected voltage in Figure 11, is selected to be fitted with the crack width, and the results are shown in Figure 12 and Equation (6).

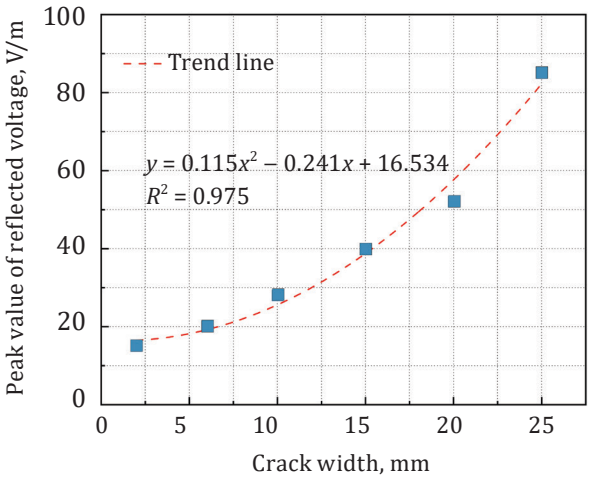

Figure 12. The relationship between a peak value of reflected voltage and crack width

$$y = 1.115x^2 - 0.24x + 16.534 (R^2 = 0.975)\,, \tag{6}$$

where y – reflected voltage at the top of the crack;
x – crack width.

Obviously, there is a clear quantitative relationship between the crack width and the echo amplitude based on Equation (6). Therefore, based on the voltage data and radar images obtained from the field detection, the width of the cracks within the pavement can be calculated by Equation (6).

5. Results and discussion

5.1. Analysis of detection results

After 3D GPR detection, the type, length, and extension depth of internal distresses of each lane were counted, and the IDR (without considering the weight) value toward each distress was calculated in Table 5.

From Table 5, it can be seen that crack is the main internal distress, while the other three distresses are relatively rare. The internal distress rate of lane 3 is all the largest. As the lane that mainly bears heavy loads, lane 3 has a high probability of internal distresses, and it is also the main maintenance object of the road department. Then, taking 100 m as the evaluation unit, Figure 13 shows the IDR value of each structural layer in lane 3. Obviously, most of the pavement internal distresses occur at the base, which is related to the typical semi-rigid base material and construction conditions in China. The reflection characteristics of the base cracks make the surface layer crack to a certain extent. The crack rate at the subbase is small because there are few cracks extending through the entire pavement structural layer. However, the loose and cavity distresses at the subbase are more prominent. This may be due to the high rainfall in the local summer, and the subbase material is prone to water damage, increasing the risk of such distresses. In addition, a small amount of poor interlayer bonding appeared in each structural layer, just proving that the distress easily occurs at the interfaces among different structural layers. In general, the internal distress types of each structural layer are different, and the damage rate is unevenly distributed.

Table 5. IDR value toward each distress of each lane from K2117 + 000 to K2119 + 500

	IDR, %			
	Crack	**Loose**	**Cavity**	**Poor interlayer bonding**
Lane 1	0.109	0.086	0.033	0.059
Lane 2	0.083	0.057	0.048	0.027
Lane 3	0.341	0.187	0.066	0.074

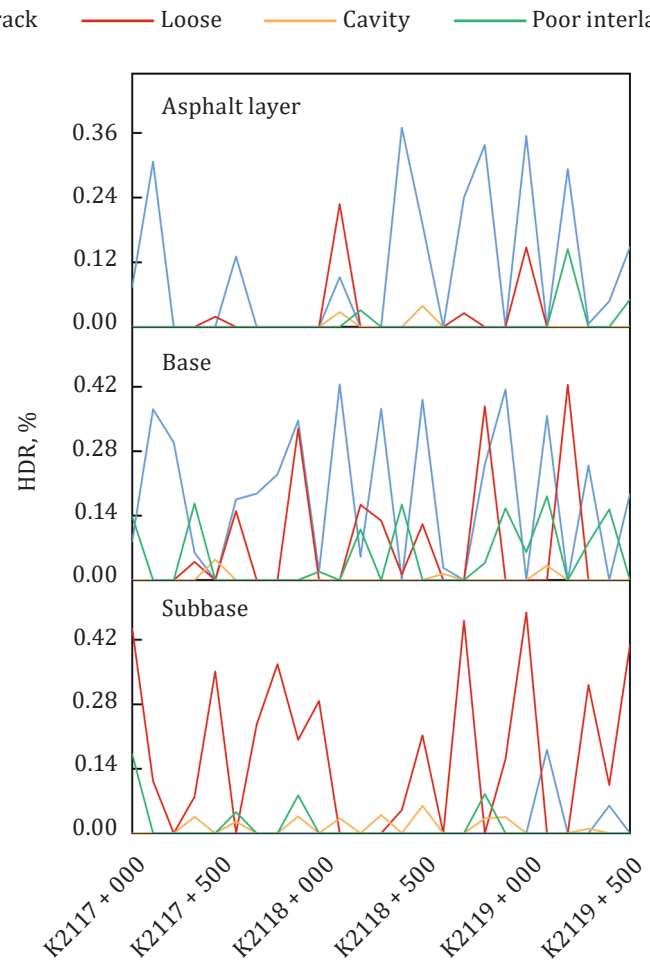

Figure 13. IDR value of each structural layer in lane 3

Figure 14 shows the overall DR and IDR of the asphalt pavement for each lane. The average DR value of the lane 3 is 1.99%, lane 1 and lane 2 are 1.01% and 1.24%, respectively. It follows that the surface distresses occur most frequently in lane 3. In addition, there are sections with DR value of 0 or IDR value of 0 in each lane, indicating that there is no direct correlation between DR and IDR. The DR value of each lane is much larger than the IDR value correspondingly on the whole, suggesting that the occurrence of internal distresses of the pavement has a lag compared to the surface distresses.

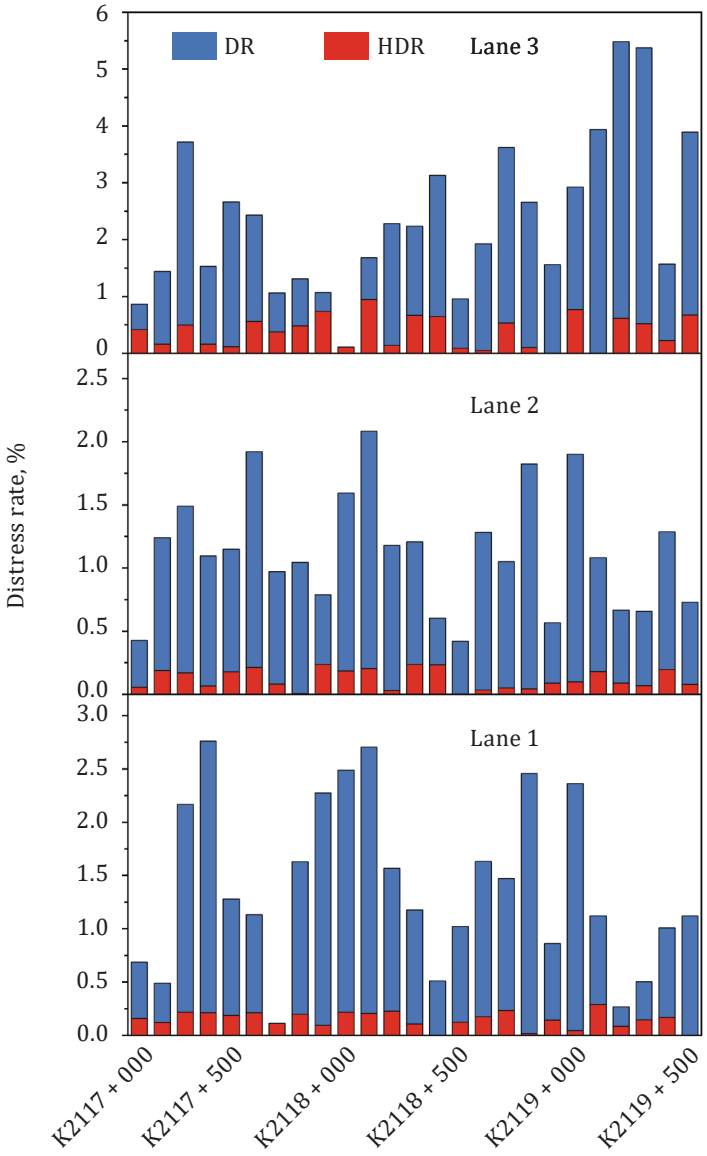

Figure 14. Overall DR and IDR of the asphalt pavement in each lane

Figure 15 shows the pavement condition index in each lane. The PICI values of lane 1 and lane 2 are all more than 90, representing excellent internal condition of pavement. The PICI value of 60% road sections in lane 3 is less than 90, showing

an overall downward trend on the internal condition of pavement. The PCI values of each lane is basically less than 90, and there are also road sections less than 80, indicating medium surface condition of the pavement. The road sections with low PCI and PICI values indicate that the damage has existed in the whole pavement structure, and the actual condition of the corresponding pavement has been poor. Obviously, it is unreasonable to use only PCI to evaluate the pavement damage condition, and the identification and analysis of the pavement internal distresses are more important to some extent. The longer service time of the existing asphalt pavement, the more types of distresses will appear within the pavement, which makes the internal damage condition worse. Therefore, the PICI model can be an important supplementary part of pavement structural damage evaluation.

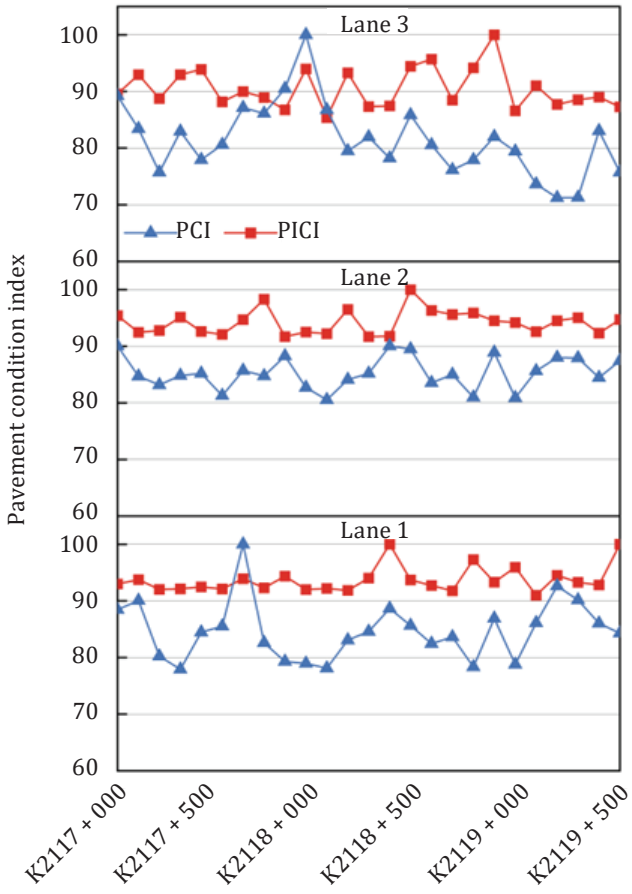

Figure 15. PCI and PICI of the asphalt pavement in each lane

5.2. Maintenance strategy based on PICI

In order to make the PICI model better serve the actual project, combined with the evaluation criteria and engineering experience, the corresponding maintenance strategies are given:

1. When PICI ≥ 90, it indicates that the internal condition of the pavement structure is good and no treatment is required.
2. When 80 ≤ PICI < 90, it indicates that there has been some degree of attenuation of the internal condition of the pavement structure, which needs to be focused on.
3. When 70 ≤ PICI < 80, it indicates that there is a certain degree of damage within the pavement structure, and structural preventive maintenance measures need to be adopted, such as overlay treatment for the original pavement, thus improving the stress state of the pavement structure and alleviating the development of internal distresses.
4. When PICI < 70, it indicates that there has been serious damage within the pavement structure, and structural reinforcement treatment is needed for the weak position, such as localized excavation and filling, or the use of grouting repair technology.

Conclusions

Based on the three-dimensional ground penetrating radar, the identification and evaluation of the internal distress of pavement have been studied, and treatment measures for maintenance under different internal damage conditions have been given, with the following specific conclusions.

- The 3D GPR system provides a real-time visualisation of internal distress through the advanced data processing software, avoiding the ambiguity of 2D GPR that uses only longitudinal profile images for recognition. Furthermore, it considers both detection depth and high resolution, which meets the requirement of quantitative evaluation of pavement structural condition.
- The forward modelling based on GprMax shows that there is a quadratic relationship between the width of the base crack and the echo amplitude, which can be used to estimate the horizontal dimension of base cracks.
- Considering the impact of the distress extension depth, two modified indices, including IDR and PICI, are proposed for the assessment of the damage status of the asphalt pavement internal structure, which can fully reflect the structural integrity of asphalt pavement.
- Most of the internal pavement structural distresses occur at the base, the subbase is mostly loose distress, and the surface layer is dominated by cracks.

Cavity distress has a lower probability of occurrence, while the poor interlayer bonding can appear in each structural layer.

In future research work, more internal distress types (such as subsidence, water-bearing abnormal area, etc.) need to be considered in order to establish more reasonable evaluation indices. Moreover, additional verification by several roads in various regions are required and affected by various traffic.

Acknowledgements

We thank the Wuhan CCCC Test, Detection and Reinforcement Engineering Co., Ltd. for providing instruments.

Funding

The research has been supported by the National Natural Science Foundation of China under Grant [number 52178437].

Disclosure Statement

The authors declare that there is no conflict of interest regarding the publication of this paper.

REFERENCES

Baili, J., Lahouar, S., Hergli, M., Al-Qadi, I. L., & Besbes, K. (2009). GPR signal de-noising by discrete wavelet transform. *NDT & E International*, *42*(8), 696–703. https://doi.org/10.1016/j.ndteint.2009.06.003

Benedetto, A., Tosti, F., Ciampoli, L. B., & D'Amico, F. (2017). An overview of ground-penetrating radar signal processing techniques for road inspections. *Signal Processing*, *132*, 201–209. https://doi.org/10.1016/j.sigpro.2016.05.016

Diamanti, N., & Redman, D. (2012). Field observations and numerical models of GPR response from vertical pavement cracks. *Journal of Applied Geophysics*, *81*, 106–116. https://doi.org/10.1016/j.jappgeo.2011.09.006

Farhan, A. H., Dawson, A. R., & Thom, N. H. (2018). Recycled hybrid fiber-reinforced & cement-stabilized pavement mixtures: Tensile properties and cracking characterization. *Construction and Building Materials*, *179*, 488–499. https://doi.org/10.1016/j.conbuildmat.2018.05.233

Feng, D. S., Wang, H. H., & Dai, Q. W. (2013). Forward simulation of Ground Penetrating Radar based on the element-free Galerkin method. *Chinese Journal of Geophysics*, *56*(1), 298–308. http://en.dzkx.org//article/doi/10.6038/cjg20130131

Giannakis, I., Tosti, F., Lantini, L., & Alani, A. M. (2019). Diagnosing emerging infectious diseases of trees using ground penetrating radar. *IEEE Transactions on Geoscience and Remote Sensing*, *58*(2), 1146–1155. https://doi.org/10.1109/TGRS.2019.2944070

Hernando, D., & del Val, M. A. (2013). A comprehensive overview on main distress mechanisms in composite pavements. *International Journal of Pavement Research and Technology*, *6*(6), 737–744. https://www.proquest.com/scholarly-journals/comprehensive-overview-on-main-distress/docview/1471042753/se-2

Iftikhar, S., Shah, P. M., & Mir, M. S. (2023). Potential application of various nanomaterials on the performance of asphalt binders and mixtures: A comprehensive review. *International Journal of Pavement Research and Technology*, *16*, 1439–1467. https://doi.org/10.1007/s42947-022-00207-5

Jing, C., Zhang, J., & Song, B. (2020). An innovative evaluation method for performance of in-service asphalt pavement with semi-rigid base. *Construction and Building Materials*, *235*, Article 117376. https://doi.org/10.1016/j.conbuildmat.2019.117376

Joshaghani, A., & Shokrabadi, M. (2022). Ground penetrating radar (GPR) applications in concrete pavements. *International Journal of Pavement Engineering*, *23*(13), 4504–4531. https://doi.org/10.1080/10298436.2021.1954182

Kırbaş, U., & Karaşahin, M. (2016). Performance models for hot mix asphalt pavements in urban roads. *Construction and Building Materials*, *116*, 281–288. https://doi.org/10.1016/j.conbuildmat.2016.04.118

Lai, W. W. L., Derobert, X., & Annan, P. (2018). A review of Ground Penetrating Radar application in civil engineering: A 30-year journey from Locating and Testing to Imaging and Diagnosis. *NDT & E International*, *96*, 58–78. https://doi.org/10.1016/j.ndteint.2017.04.002

Leng, Z., & Al-Qadi, I. L. (2014). An innovative method for measuring pavement dielectric constant using the extended CMP method with two air-coupled GPR systems. *NDT & E International*, *66*, 90–98. https://doi.org/10.1016/j.ndteint.2014.05.002

Li, S., Gu, X., Xu, X., Xu, D., Zhang, T., Liu, Z., & Dong, Q. (2021). Detection of concealed cracks from ground penetrating radar images based on deep learning algorithm. *Construction and Building Materials*, *273*, Article 121949. https://doi.org/10.1016/j.conbuildmat.2020.121949

Liang, X., Yu, X., Chen, C., Jin, Y., & Huang, J. (2022). Automatic classification of pavement distress using 3D ground-penetrating radar and deep convolutional neural network. *IEEE Transactions on Intelligent Transportation Systems*, *23*(11), 22269–22277. https://doi.org/10.1109/TITS.2022.3197712

Liu, H., & Sato, M. (2014). In situ measurement of pavement thickness and dielectric permittivity by GPR using an antenna array. *NDT & E International*, *64*, 65–71. https://doi.org/10.1016/j.ndteint.2014.03.001

Liu, Z., Sun, T., Huang, T., Liu, G., Tao, Y., Wang, G., & Wang, L. (2023). Forward modeling and model test of ground-penetrating radar toward typical asphalt pavement distresses. *Advances in Civil Engineering*, *2023*. https://doi.org/10.1155/2023/2227326

Muller, W. B. (2020). Semi-automatic determination of layer depth, permittivity and moisture content for unbound granular pavements using multi-offset 3-D GPR. *International Journal of Pavement Engineering*, *21*(10), 1281–1296. https://doi.org/10.1080/10298436.2018.1539485

Obaidat, M. T., & Al-Kheder, S. A. (2006). Integration of geographic information systems and computer vision systems for pavement distress classification. *Construction and Building Materials*, *20*(9), 657–672. https://doi.org/10.1016/j.conbuildmat.2005.02.009

Wang, Y., Ni, F. J., & Ma, X. (2008). Stress comparison of asphalt pavements with different base crack states. *Journal of Traffic and Transportation Engineering*, *8*(6), 34–39. https://transport.chd.edu.cn/en/article/id/200806007

Xiong, X., & Tan, Y. (2023). Deep learning-based detection of tie bars in concrete pavement using ground penetrating radar. *International Journal of Pavement Engineering*, *24*(2), Article 2155648. https://doi.org/10.1080/10298436.2022.2155648

Xiong, X., Meng, A., Lu, J., Tan, Y., Chen, B., Tang, J., Zhang, C., Xiao, S., & Hu, J. (2024a). Automatic detection and location of pavement internal distresses from ground penetrating radar images based on deep learning. *Construction and Building Materials*, *411*, Article 134483. https://doi.org/10.1016/j.conbuildmat.2023.134483

Xiong, X., Tan, Y., Hu, J., Hong, X., & Tang, J. (2024b). Evaluation of asphalt pavement internal distresses using three-dimensional ground-penetrating radar. *International Journal of Pavement Research and Technology*, *2024*, 1–12. https://doi.org/10.1007/s42947-023-00402-y

Xiong, X., Xiao, S., Tan, Y., Zhang, X., Zhang, D., Han, M., & Wang, W. (2021). Estimation of density and moisture content in asphalt mixture based on dielectric property. *Construction and Building Materials*, *298*, Article 123518. https://doi.org/10.1016/j.conbuildmat.2021.123518

Zhou, L., Ni, F., & Leng, Z. (2014). Development of an asphalt pavement distress evaluation method for freeways in China. *International Journal of Pavement Research and Technology*, *7*(2), 159–167. https://www.proquest.com/scholarly-journals/development-asphalt-pavement-distress-evaluation/docview/1514887712/se-2